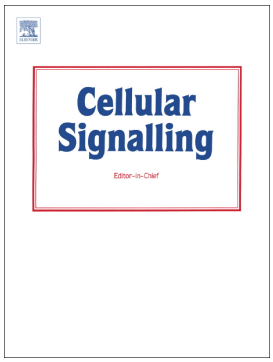

The allosteric site regulates the voltage sensitivity of muscarinic receptors

Anika Hoppe, Maria Marti-Solano, Matthäus Drabek, Moritz Bünemann, Peter Kolb, Andreas Rinne

PII: S0898-6568(17)30279-6
DOI: doi:10.1016/j.cellsig.2017.10.011
Reference: CLS 9019

To appear in: *Cellular Signalling*

Received date: 8 June 2017
Revised date: 28 September 2017
Accepted date: 19 October 2017

Please cite this article as: Anika Hoppe, Maria Marti-Solano, Matthäus Drabek, Moritz Bünemann, Peter Kolb, Andreas Rinne , The allosteric site regulates the voltage sensitivity of muscarinic receptors. The address for the corresponding author was captured as affiliation for all authors. Please check if appropriate. Cls(2017), doi:10.1016/j.cellsig.2017.10.011

The allosteric site regulates the voltage sensitivity of muscarinic receptors

Anika Hoppe[a], Maria Marti-Solano[b], Matthäus Drabek[b], Moritz Bünemann[c], Peter Kolb[b] and Andreas Rinne[a,*]

[a]Department of Cardiovascular Physiology, Ruhr-University Bochum, Universitätsstr. 150, 44780 Bochum, Germany

[b]Department of Pharmaceutical Chemistry, Philipps-University Marburg, Marbacher Weg 6-10, 35032 Marburg, Germany

[c]Department of Pharmacology and Clinical Pharmacy, Philipps-University Marburg, Karl-von-Frisch-Str. 1, 35043 Marburg, Germany

[*]Corresponding author

E-mail address: andreas.rinne@rub.de

Abbreviations:

4-(4-Butyl-1-piperidinyl)-1-(2-methylphenyl)-1-butanone hydrochloride (AC-42), acetylcholine (ACh), allosteric modulator (AM), Benzyl quinolone carboxylic acid (BQCA), extracellular loop (ECL), Förster resonance energy transfer (FRET), Function – voltage curve (F-V curve), G protein-coupled receptor (GPCR), membrane potential (V_M), molecular dynamics (MD), muscarinic M_1-receptor (M_1-R), muscarinic M_3 receptor (M_3-R), positive allosteric modulator (PAM), negative allosteric modulator (NAM), transmembrane helical domain (TM).

Abstract

Muscarinic receptors (M-Rs) for acetylcholine (ACh) belong to the class A of G protein–coupled receptors. M-Rs are activated by orthosteric agonists that bind to a specific site buried in the M-R transmembrane helix bundle. In the active conformation, receptor function can be modulated either by allosteric modulators, which bind to the extracellular receptor surface or by the membrane potential via an unknown mechanism. Here, we compared the modulation of M_1-Rs and M_3-Rs induced by changes in voltage to their allosteric modulation by chemical compounds. We quantified changes in receptor signaling in single HEK 293 cells with a FRET biosensor for the G_q protein cycle. In the presence of ACh, M_1-R signaling was potentiated by voltage, similarly to positive allosteric modulation by benzyl quinolone carboxylic acid. Conversely, signaling of M_3-R was attenuated by voltage or the negative allosteric modulator gallamine. Because the orthosteric site is highly conserved among M-Rs, but allosteric sites vary, we constructed "allosteric site" M_3/M_1-R chimeras and analyzed their voltage dependencies. Exchanging the entire allosteric sites eliminated the voltage sensitivity of ACh responses for both recepotrs, but did not affect their modulation by allosteric compounds. Furthermore, a point mutation in M_3-Rs caused functional uncoupling of the allosteric and orthosteric sites and abolished voltage dependence. Molecular dynamics simulations of the receptor variants indicated a subtype-specific crosstalk between both sites, involving the conserved tyrosine lid structure of the orthosteric site. This molecular crosstalk leads to receptor subtype-specific voltage effects.

Keywords

GPCRs, Muscarinic Receptors, voltage dependence, allosteric regulation

1. Introduction

Muscarinic receptors for acetylcholine belong to the class A of the family of seven transmembrane (TM) or G protein-coupled receptors (GPCRs). The activation of these receptors is induced by ligands that bind to an orthosteric site that is accessible from the extracellular milieu and lies buried inside the seven transmembrane helices. Binding of agonists to this site favors active receptor conformations, which transmit signals through interaction with intracellular G proteins (Kruse et al., 2012). In addition to the activation elicited by orthosteric agonists, other ligands can modulate receptor function by binding to allosteric binding sites located at the extracellular receptor surface (allosteric modulators [AMs]). In particular, the extracellular loops (ECL) 2 and 3 as well as amino acid residues in TM 7 are involved in binding of AMs (this site is termed "allosteric site" in this paper) (Conn et al., 2009; Thal et al., 2016). AMs either potentiate (positive allosteric modulators, PAMs) or attenuate (negative allosteric modulators, NAMs) receptor signaling. Binding of an AM induces a conformational change of the allosteric site, which transduces to the orthosteric binding site, modifying agonist binding (ligand affinity) and/or the receptor's ability to activate G proteins (signaling efficacy) (Bock et al., 2012; Shivnaraine et al., 2016).

In addition, the activity of some GPCRs depends on the membrane potential. For muscarinic receptors (M-Rs) such a voltage dependence was initially discovered in M_2-Rs, which showed reduced agonist binding and activation at positive membrane potentials (Ben-Chaim et al., 2003; Ben-Chaim et al., 2006). This has motivated further studies and we now know that the properties of voltage sensitivity depend also on the interaction pattern of the orthosteric ligand with the receptor. For example, a depolarization of the membrane increased the function of M_2-Rs, if choline or pilocarpine were used as agonists, but caused deactivation of M_2-Rs following ACh exposure (Navarro-Polanco et al., 2011; Moreno-Galindo et al., 2016). At the same time, the direction (or polarity) of the voltage effect for a given agonist differs with the receptor subtype: Whereas depolarization caused activation of M_1-Rs, structurally related M_3-Rs were deactivated in the presence of ACh or carbachol (Rinne et al., 2015). The observation that the different interaction capacity of allosteric compounds determines whether they act as PAM or NAM ("probe

dependency") is a hallmark of allostery in GPCRs (Wootten et al., 2013). This led us to hypothesize that voltage can be regarded as an allosteric modulator of receptor function. To test this experimentally, we compared the effect that voltage has on signaling of M_1-Rs, M_3-Rs and M_3-R/M_1-R chimeras to the modulation of receptor function by allosteric compounds. We used fluorescence resonance energy transfer (FRET) to monitor activation of unlabeled receptors with a G_q protein biosensor and whole cell voltage clamp to quantify their voltage sensitivity. Modifications of the allosteric site of M_3-Rs, either by exchange of extracellular M_3-R regions with corresponding M_1-R regions or by a point mutation that causes functional uncoupling of the allosteric site, eliminated the voltage sensitivity in the presence of ACh. Furthermore, mutations of the conserved orthosteric tyrosine lid of M_3-Rs turned receptor inactivation by voltage into activation. To analyze the molecular contribution of both receptor regions to the mechanism of voltage dependence, we assessed the behavior of wild type receptors, chimeras and mutant receptors with molecular dynamics (MD) simulations. Collectively, our experimental data and MD simulations demonstrate for the first time that the allosteric site has a significant contribution to voltage dependence in M-Rs. In particular, a receptor subtype-specific crosstalk of the allosteric site with the orthosteric tyrosine lid controls voltage dependence of M-Rs.

2. Materials and methods

2.1 Molecular Biology and cell culture

To generate synthetic chimeras of muscarinic receptors, cDNA fragments of M_1-R were generated by PCR and inserted into the cDNA of M_3-R using the In-Fusion cloning method (Clontech) with pcDNA3 (Invitrogen) as a plasmid backbone. The following receptor constructs were generated: M_1/M_3-R chimera: The amino acids (aa) 1 to 164 of M_1-R, encoding for the N terminus and TM 1 to TM 4, were fused to aa 208 to 590 of M_3-R, encoding for ECL 2, TM 5 to TM 7 and the C terminus. M_3-BQCA-R: The fragments aa 208 to 229 (ECL 2), aa 514 to 527 (ECL 3) and aa 528 to 547 (TM 7) of M_3-R were substituted with aa 165 to 186 (ECL 2), aa 388 to 401 (ECL 3) and aa 402 to 421 (TM 7) of M_1-R, respectively. Other chimeras: Single substitutions of ECL 2, ECL 3 and TM 7 of M_3-R to the corresponding cDNA frag-

ments of M_1-R, or combinations of two fragments, as indicated in the text. The mutant receptors M_3-R ($W^{7.35}A$) and M_3-R (FFF) were generated by PCR. FFF refers to the triple mutation $Y^{333}F$, $Y^{6.51}F$ and $Y^{7.39}F$. The aa positions refer to entries NP_000729 (human M_1-R) and NP_000731 (human M_3-R) of the NCBI protein data base. All constructs were verified by DNA-sequencing.

All experiments were performed using HEK 293 cells that were grown in Dulbecco's modified eagle medium (DMEM), supplemented with glutamine, with fetal calf serum and with penicillin/streptomycin using standard cell culture protocols. Cell culture medium and supplements were purchased from Gibco. HEK 293 cells were transiently transfected using Effectene reagent (Qiagen) according to the manufacturer's instructions and the following cDNAs (amount in µg per 3 cm culture-dish): M_1-R, M_3-R, mutant receptors or chimeras (1.0), $G\alpha_q$-YFP (1.0), $G\beta_1$-Cerulean (0.5), $G\gamma_2$ (0.2) and GPCR kinase 2 (0.5). All cDNAs were subcloned into pcDNA1 or into pcDNA3 plasmids (Invitrogen). Experiments were performed 48 to 72 hours after transfections.

2.2 Fluorescence microscopy

Fluorescence was measured using single HEK 293 cells seeded on Poly-L-lysine-coated glass cover slips. The cells were mounted on an inverted microscope (Zeiss Axiovert 200, oil immersion objective 100x/1.4), equipped with a Polychrome V monochromatic illumination source and a photodiode-based dual emission photometry system suitable for collecting CFP and YFP emissions (TILL Photonics). Cells were excited at λ = 435 nm (excitation filter: D420/20, beam splitter DCLP 460) with short light pulses to minimize photo bleaching (pulse duration 10 ms to 50 ms, the frequency of illumination was 5 Hz). Corresponding emitted fluorescence stemming either from CFP (F_{CFP}, emission filter: D480/40) or from YFP (F_{YFP}, emission filter LP 515) were acquired simultaneously (beam splitter: DCLP 505). FRET was defined as ratio F_{YFP}/F_{CFP}. All optical filters and beamsplitters were from Chroma or Semrock. Fluorescent signals were digitized and stored using a hardware/software package from HEKA (EPC10 amplifier and Patchmaster software).

To obtain concentration-response relationships of the different receptor constructs for the agonists used (Figure S1), the FRET responses at test concentrations were normalized to the maximal response at a saturating concentration (i.e. $FRET/FRET_{100\ \mu M}$ for ACh and $FRET/FRET_{1mM}$ for Pilocarpine). To obtain EC_{50} values, these data were plotted against the agonist concentrations. Curve fitting and calculations of EC_{50} values were performed using an implemented function of Graphpad Prism software (version 5.0). For other experiments, traces were normalized to the initial ratio value before agonists were applied ($FRET/FRET_0$, denoted as FRET normalized).

To quantify the voltage dependencies of different receptor constructs, we tried to reach comparable levels of pre-activation of the receptor/G_q signal by applying an agonist concentration that reflects the corresponding EC_{50} value for each chimera or mutant receptor (Figure S1).

Data to quantify the magnitude of the voltage effect are shown as normalized changes of FRET (ΔFRET, normalized). For normalization, the base line was defined as the FRET signal before agonist application (Δ FRET = 0) and the FRET level at -90 mV was defined as 100 % (Δ FRET = 1), just before the voltage step was applied.

To obtain function-voltage curves (F-V curves, Figure 7), each receptor or chimera was pre-activated to a level of 50 % with ACh and subjected to several test potentials. To obtain F-V curves, subsequent changes in FRET were normalized to the FRET response at -90 mV ($FRET/FRET_{-90mV}$) and plotted against V_M. The data were fitted to a sigmoidal Boltzmann function implemented in Graphpad Prism software (version 5.0) to obtain V_{50} values. V_{50} is defined as the membrane potential V_M that causes 50 % change in receptor signaling.

2.3 Solutions and Chemicals

During all experiments, cells were superfused with Hepes-buffered solution (HBS) or with HBS containing agonists. The solutions were rapidly exchanged using a customized, gravity-driven superfusion system that was operated by solenoid valves. The extracellular HBS contained (in mM): NaCl 137; KCl 5.4; $CaCl_2$ 0.5; $MgCl_2$ 1.0; Hepes 10.0, pH 7.3. The intracellular HBS contained (in mM): K-aspartate 100; KCl 40; NaCl 5.0, $MgCl_2$ 5.0; ATP 5.0; EGTA 2.0; GTP 0.025; HEPES/KOH 20.0, pH 7.3. Standard chemicals were from Merck. ACh, BQCA, gallamine and pilocarpine were from Sigma-Aldrich.

2.4 Whole cell voltage clamp

The membrane potential (V_M) was controlled using whole-cell voltage clamp. Patch pipettes were fabricated from borosilicate glass and were filled with intracellular HBS (final resistance 5-10 MΩ). V_M was clamped using a patch clamp amplifier (List LM/EPC 7) and controlled by a commercial hardware/software package (ISO2, MFK, Frankfurt/Main, Germany). FRET was recorded simultaneously as described above.

2.5 Molecular Dynamics (MD) Simulations

In order to generate the different systems used for MD simulations, the sequences of the human M_1-R (P11229) and the human M_3-R (P20309) were retrieved from Uniprot and used to build an activated receptor model based on the crystallized structure of the nanobody-stabilized M_2-R in complex with the agonist iperoxo (PDB ID 4MQS) (Kruse et al., 2013) using the MOE software and default conditions (Molecular Operating Environment (MOE) software, http://www.chemcomp.com/software.htm). We also produced a chimeric receptor variant corresponding to M_3-BQCA-R using the mutate function present in MOE. The same function was used to introduce the $W^{7.35}$A point mutation in the activated M_3-R model. The resulting four activated receptor structures were used to dock the agonist ACh using the binding mode generated by a previously established protocol (Rinne et al., 2015). The protonation state of titratable groups was predicted for a pH value at 7.4 based on PROPKA (Li et al., 2005) and, in order to

preserve the active conformation of the receptors, residue $D^{2.50}$ was kept in its protonated neutral form and a 10-amino acid C-terminal G_q protein fragment was modeled in the intracellular receptor region based on the crystal structure of the β_2-adrenergic receptor in complex with G_s (PDB ID 3SN6). The resulting systems were embedded in a hydrated (water phase containing 0.15 M NaCl) 80 x 80 POPC bilayer using the CHARMM-GUI system builder (Wu et al., 2014), which was also used to generate ACh parameters with Antechamber. Three replicates of each of the resulting ≈35000 atom systems were then independently equilibrated using the six step Namd protocol for membrane proteins provided by the CHARMM-GUI system builder and later run under NVT conditions using the ACEMD software (Harvey et al., 2009). These production runs were run at 300K with a time-step of 4 fs and a hydrogen-scaling factor of 4. Non-bonded interactions had a cutoff at 9 Å and a smooth switching function of 7.5 Å. The long-range electrostatics used the PME methodology with a grid spacing of 1 Å. For all four different receptor systems, the three independently generated replicates were run for 400 ns each reaching an accumulated simulation time of 1.6 μs. In order to confirm the stability of the systems, protein RMSDs over the simulation time – excluding hydrogen atoms – were calculated using the RMSD Trajectory Tool plugin present in VMD 1.9.2 (Figure S2).

2.6 Statistical Analysis

Data are presented as individual observations or as summarized data (mean ± SEM of n individual cells). Statistical analysis was performed using Student's t-test and differences at the level of $P < 0.05$ were considered significant.

3. Results

3.1 Changes of M-R function by voltage or by allosteric modulation

We analyzed the voltage sensitivities of M_1-Rs and M_3-Rs in single voltage-clamped HEK 239 cells expressing a biosensor, which reports receptor signaling based on the dissociation of fluorescently labeled subunits of heterotrimeric G_q proteins (termed G_q biosensor) (Hoffmann et al., 2012; Rinne et al., 2015).

As depicted in Figure 1A, application of 20 nM ACh to HEK 293 cells expressing the M_1-R and the G_q biosensor caused a rapid decrease in the FRET ratio (F_{YFP}/F_{CFP}), indicating an activation of M_1-R and G_q. A depolarization step from -90 mV to +40 mV potentiated M_1-R activity, although the concentration of ACh was kept constant. This effect was reversible as V_M returned to -90 mV (Figure 1A, upper panel). To compare this effect to allosteric modulation, we used benzyl quinolone carboxylic acid (BQCA), which increases the receptor's affinity for ACh (Shirey et al., 2009). The PAM BQCA potentiated M_1-R/G_q signaling in cells that were exposed to ACh, but not voltage-clamped (Figure 1B, upper panel). When BQCA was applied for 60 s, the activity change of M_1R was similar to the one induced by voltage. Figures 1C and 1D show the corresponding experiments for the M_3-R. An application of 20 nM ACh to HEK 293 cells expressing M_3-Rs induced an activation of M_3-R/G_q at -90 mV. In sharp contrast to M_1-R, depolarization to +40 mV caused deactivation of M_3-R and G_q (Figure 1C, upper panel). To compare this effect to negative allosteric modulation, we used the NAM gallamine, which reduces the receptor's affinity for ACh (Ehlert and Griffin, 2008). Indeed, a co-application of gallamine (100 µM) for 60 s reduced M_3-R signaling in the presence of 20 nM ACh (Figure 1D, upper panel). Again, this inhibitory effect was similar to the one induced by voltage. These effects were not restricted to ACh and also observed for the agonists carbachol and iperoxo (Figure S3). For both receptor subtypes, neither a depolarization of the membrane nor the corresponding allosteric compounds altered receptor signaling in the absence of ACh (Figure 1 A through D, lower panels). These data suggest that voltage and allosteric modulators can have the same effect on receptor function. We were then interested to test, if binding of an AM to the allosteric site competes with voltage dependence. To test this, we pre-activated the M_1-R with ACh and BQCA and subjected the cells to a depolarization of the membrane. As shown in Figure 2, binding of BQCA did not affect the voltage dependence of the receptor at two different concentrations of the PAM, suggesting that occupancy of the allosteric site does not interfere with voltage sensitivity of M-Rs.

3.2 Pharmacological characterization of allosteric M_3/M_1 receptor chimeras

Because voltage and the studied AMs have the same effect on receptor function (Figure 1), we were interested to test if the extracellular allosteric site itself would influence the voltage dependence of M-Rs. The orthosteric binding site for ACh is highly conserved among all five muscarinic receptor subtypes, but extracellular regions, including the allosteric site, are more variable and specific for each receptor subtype (Kruse et al., 2012; Thal et al., 2016). This has allowed the develop allosteric compounds that are specific for a particular muscarinic receptor subtype: for example, the PAM BQCA is highly selective for M_1-Rs, because it interacts with amino acid residues of the extracellular allosteric site, which are not present in other M-R subtypes (Abdul-Ridha et al., 2014b). In line with this binding preference, we observed a potentiation of ACh/G_q-signaling by BQCA only for the M_1-R (Figure 3A), but not for the M_3-R (Figure 3B). To test if the extracellular allosteric site is involved in voltage sensitivity, we generated an allosteric M_3-R receptor chimera that binds BQCA, termed M_3-BQCA-R. This chimera contains ECL 2, ECL 3 and TM 7 stemming from M_1-R (cartoon in Figure 3C). The chimera acquired sensitivity to BQCA and showed a clearly detectable potentiation of ACh/G_q signaling (Figure 3C). This response indicated that the chimera was functional in terms of orthosteric activation by ACh and allosteric modulation by a PAM. The subsequent analysis of "partial allosteric" chimeras revealed that only constructs that had received ECL 3 were sensitive to BQCA (Figure 4A through 4D).

3.3 Voltage dependence of allosteric M_3/M_1 receptor chimeras

To compare the extent of the voltage effect between M_3-R and the chimeras, we applied ACh in nominal concentrations corresponding to the EC_{50}-value for each construct (see Figure S1) and normalized the data to the activation level at -90 mV, right before the depolarizing step was applied. The voltage response of wild type M_3-Rs is given as a reference (dashed line, mean values taken from Figure 1C). Our experiments revealed that M_3-BQCA-R, which contained the entire allosteric site from M_1-R, was almost insensitive to voltage (Figure 5A). All other chimeras showed a pronounced voltage sensitivity (Figures 5B through E). However, those chimeras that were sensitive to BQCA (see above) displayed a significant

reduction in voltage dependence (summarized data in Figure 5F). These data demonstrate that the allosteric site affects the voltage sensitivity of M_3-Rs. The fact that M_3-BQCA-R did not show the original M_1-R phenotype (activation) shows that voltage also affects different receptor regions in addition to the allosteric site.

The influence of the allosteric site on voltage sensitivity was underscored by a "reversed chimera", which was based on TM 1 to TM 4 of M_1-R and TM 5 to TM 7 of M_3-R, thus representing an M_1-R that contains the entire allosteric site of the M_3-R (Figure 6A). The functional transfer of the allosteric site stemming from M_3-R was evident by a modified gallamine response (Figure 6B). In comparison to the M_1-R, which has a higher affinity for gallamine than M_3- or M_5-R subtypes (Gnagey et al., 1999), the chimera was less sensitive and the extent of the gallamine response was similar to M_3-Rs (summary data in Figure 6C). The M_1/M_3-R chimera did not show any detectable voltage sensitivity during depolarization to +40 mV (Figure 6D and F-V curve in Figure 8). These data demonstrate that the allosteric site modulates the voltage dependence of M-Rs in a receptor subtype-specific fashion.

3.4 Functional uncoupling of the allosteric site disrupts the voltage dependence of ACh-activated M_3-Rs

Analysis of the allosteric epitope of M_2-Rs has identified a conserved tryptophan residue ($W^{7.35}$) at the ECL 3/TM 7 interface that is essential for binding of allosteric modulators (Prilla et al., 2006). For M_2-Rs, the point mutation $W^{7.35}A$ prevented binding of allosteric modulators and, more important for the present study, disrupted the cooperativity of allosteric and orthosteric binding sites. To analyze the impact of this cooperativity on voltage dependence, we introduced the corresponding mutation in the M_3-R ($W^{7.35}A$). As depicted in Figure 7A, the mutant receptor responded to ACh and showed activation of G_q, but was almost insensitive to gallamine. When the membrane potential was changed from -90 mV to +40 mV, there was no detectable change in activity during depolarization (Figure 7B). This result confirms that the mechanism of voltage dependence in ACh-activated M-Rs requires a crosstalk of allosteric and orthosteric sites. To further analyze chimeras or mutant receptors that displayed reduced voltage sensitivi-

ty, we generated receptor function-voltage (F-V) curves. As depicted in Figure 8A and 8B, the F-V curves of both parental receptors had a sigmoidal shape following a Boltzmann distribution. The V_{50}-values derived from these curves were in the physiological range of membrane potential changes (M_1-R: -51 mV, M_3-R: -42 mV) and z-values were around 1 (M_1-R: z = 1.07, M_3-R: z = 0.65). In contrast, the properties of M_3-BQCA-R were altered: Voltage dependence was detectable but strongly reduced as shown by a flat sigmoidal curve with V_{50} shifted to -89 mV (Figure 8B). In the two remaining constructs, the M_1/M_3 allosteric chimera (Figure 8A) and M_3-R (W7.35A) (Figure 8B), voltage dependence was completely lost. The corresponding F-V-curves were linear with no detectable activity changes. These data show that the allosteric site affects the voltage sensitivity of M-Rs over a wide range of V_M. The two remaining open questions are (i) How does the allosteric site interact with the orthosteric site and (ii) Does the allosteric site contain a voltage sensor in M-Rs?

3.5 Structural analysis of M_1-R and M_3-R activation

To address the first question, we focused on those regions of the orthosteric site that are in close proximity to the extracellular allosteric site. A comparison of crystal structures obtained from inactive and active M-Rs has revealed the orthosteric site residues responsible for interactions with agonists during receptor activation (Kruse et al., 2013). Among them, the authors have identified three conserved tyrosines ($Y^{3.33}$, $Y^{6.51}$ and $Y^{7.39}$), which are located at the interface between the orthosteric and the allosteric sites. During receptor activation, the tyrosine residues form a lid-like structure right above the orthosteric site. The resulting closure of the orthosteric site by this tyrosine lid appears to be crucial for agonist binding and subsequent activation of M-Rs. Interestingly, this tyrosine lid has also been implicated in a putative mechanism to sense voltage in the M_2-R (Barchad-Avitzur et al., 2016). To analyze how the different allosteric regions of M_1-R and M_3-R may affect receptor conformations, we performed MD simulations and focused on the communication between the allosteric site and the tyrosine lid region. To do so, we generated 3D structural models of M_1-R, M_3-R, M_3-BQCA-R and M_3-R ($W^{7.35}A$) in active-like conformations based on the crystal structure of the nanobody-stabilized M_2-R in complex with the agonist

iperoxo (4MQS). The resulting four receptor structures in an activated conformation were then used to dock the agonist ACh to the orthosteric binding site using a previously established protocol (Rinne et al., 2015) and later embedded in a hydrated and ionized POPC bilayer using the CHARMM-GUI system builder (Wu et al., 2014). The resulting systems were run in three replicates of 400 ns each using the ACEMD software (Harvey et al., 2009), reaching an accumulated simulation time of 1.6 μs.

The results of these simulations are presented in Figure 9, with Figure 9A showing the location of the analyzed region connecting ECL 2 and the orthosteric ACh-binding site. A detailed analysis of this region (Figures 9B through 9E) showed that the tyrosine lid can adopt a different set of conformations depending on the receptor species: Simulations for the M_1-R showed that the tyrosine lid remained in the closed state with $Y^{3.33}$, $Y^{6.51}$ and $Y^{7.39}$ stabilized by hydrogen bonds (Figure 9B). In contrast, the tyrosine lid of the M_3-R was less stable, alternating between a closed conformation and a more unstable, partially open conformation (Figure 9C). This instability seemed to be correlated to a different rotameric state of residue $W^{7.35}$, which is found directly on top of $Y^{7.39}$. In the M_1-R, $W^{7.35}$ adopted a conformation parallel to the membrane plane (Figure 9B), while in case of the M_3-R we observed an alternative orientation of $W^{7.35}$, perpendicular to the membrane (Figure 9C). Each particular orientation of $W^{7.35}$ had a direct effect on the closed or open state of the tyrosine lid. Interestingly, the orientation of the tryptophan itself was directly influenced by equivalent residues of ECL 2 belonging to the allosteric site, namely Y179 for the M_1-R and F222 for the M_3-R (Figures 9B and 9C, respectively). Remarkably, this particular position of ECL 2 has been described as key for the allosteric effects of BQCA (Abdul-Ridha et al., 2014a) and for the subtype selectivity of gallamine among M-R species (Huang et al., 2005). In the case of the M_1-R, we found that Y179 could adopt two different conformations: In the most frequent one, it pointed up towards the extracellular milieu, while in an alternative conformation it established an edge-to-face orientation with $W^{7.35}$ (Figure 9B). In both cases, $W^{7.35}$ adopted the aforementioned orientation parallel to the membrane that stabilized the closed conformation of the tyrosine lid (Figure 9B). In the M_3-R the corresponding residue F222 showed an entirely different orientation, pointing downwards to the helix bundle of the receptor (Figure 9C). This resulted in F222 alternating between two orientations. The first one was an

edge-to-face orientation with $W^{7.35}$, in which the "edge" of $W^{7.35}$ contacts the "face" of F222. This conformation was similar to the one observed for Y179 in the M_1-R, therefore stabilizing the tyrosine lid. The alternative orientation established an interaction with $W^{7.35}$, in which the F222 "edge" interacts with the $W^{7.35}$ "face". This second interaction stabilized $W^{7.35}$ in an orientation perpendicular to the membrane surface, which resulted in a destabilized tyrosine lid with a partially open conformation (Figure 9C). This was reflected by a drop in interaction frequency of $Y^{3.33}$ and $Y^{7.39}$ over the simulated time – measured as distance between OH-groups lower than 4.5 Å- from 79 % in the M_1-R to 58 % in the M_3-R.

The remaining two systems – the chimera M_3-BQCA-R and the mutant M_3-R ($W^{7.35}$A) – confirmed the observations made in the two wild type receptors. M_3-BQCA-R contained the allosteric site of the M_1-R and therefore introduced a tyrosine residue equivalent to Y179 in ECL 2. The presence of Y179 had a similar effect on the orientation of $W^{7.35}$ as the one seen for the M_1-R and stabilized the tyrosine lid in its closed conformation (compare Figures 9B and 9D). This changed orientation resulted in an intermediate frequency in $Y^{3.33}$ -$Y^{7.39}$ interactions of 62 %. In the fourth system, we analyzed the effect of the mutation $W^{7.35}$A on the tyrosine lid of the M_3-R (Figure 9E). MD simulations using the mutant M_3-R clearly showed that F222 in ECL 2 had higher flexibility, alternating between multiple orientations. Consequently, the stabilization of the tyrosine lid was lost, with a $Y^{3.33}$- $Y^{7.39}$ interaction frequency of only 0.19 %, effectively causing the uncoupling of orthosteric and allosteric binding sites.

3.6 The role of the tyrosine lid in the voltage dependence of M_3-Rs.

Our MD simulations revealed that the allosteric site may interfere with the orthosteric tyrosine lid. A recent study has linked the tyrosine residues to voltage dependence and proposed that the tyrosine lid serves as a voltage sensor within the orthosteric site of M-Rs (shown for the M_2-R in (21)). This concept appears reasonable, because the tyrosine residues are exposed to the electrical field across the membrane and represent dipole moments that are sensitive to potential changes. Therefore, we were interested in assessing whether the tyrosine lid would also serve as a voltage sensor in the M_3-R. To address this, we generated a triple mutant, in which the three tyrosine residues of the lid structure at positions 3.33, 6.52

and 7.39 were mutated to phenylalanine, termed M_3-R (FFF). This particular substitution removes the largest part of the voltage sensing dipole moments and the possibility to interact via hydrogen bonds while preserving the structure of the lid (Barchad-Avitzur et al., 2016). When subjected to ACh and membrane depolarization, M_3-R (FFF) displayed a clearly detectable voltage sensitivity (Figure 10A). Interestingly, it responded to depolarization of the membrane with activation. This change in polarity of the voltage effect has been only observed in M_3-Rs that were activated by the partial agonist pilocarpine instead of ACh (Figure 10B). Such a probe dependency of the voltage effect was demonstrated previously for pilocarpine-activated M_2-Rs (Navarro-Polanco et al., 2011) and M_3-Rs (Rinne et al., 2015) and has been attributed to divergent agonist binding modes capable of stabilizing agonist-specific receptor conformations with varying voltage sensitivities (Rinne et al., 2015). To analyze whether the voltage dependence of the pilocarpine-bound M_3-R conformation was affected by the allosteric site, we exposed M_3-BQCA-R and M_3-R ($W^{7.35}A$) to pilocarpine. The mutant receptor M_3-R ($W^{7.35}A$) and the chimera M_3-BQCA-R, which were voltage insensitive in the ACh-bound conformation, showed a clearly detectable voltage dependence at +40 mV, comparable to wild type M_3-Rs (Figures 10C and 10D). Taken together, these data show that regulation of voltage dependence by the allosteric site is agonist-dependent. Moreover, neutralization of the dipole moments of the tyrosine lid does not abolish the voltage sensitivity, but reverses the polarity of the voltage effect. Therefore, it is unlikely that the allosteric site contributes to voltage sensitivity by directly acting as a voltage sensor, as the pilocarpine experiments suggest. This indicates that additional, still unknown receptor regions can contribute to the voltage sensitivity of M-Rs.

4. Discussion

4.1 The allosteric site affects voltage dependence of M-Rs

This study was motivated by comparing the modulation of receptor function by V_M with classical AMs (Figures 1 and 2). The membrane potential modulates pre-activated M-Rs to alter receptor function, a property that is shared with most chemical AMs (Wootten et al., 2013). The modulation of ACh-activated M-Rs by V_M was affected by the same extracellular receptor region that binds AMs: We identi-

fied ECL 2, ECL 3 and TM 7 as important structures affecting voltage dependence of M-Rs (Figures 3 through 6). The modulation of M-Rs by AMs relies on the same structures, as compounds for M_1-Rs (Abdul-Ridha et al., 2014a), M_2-Rs and M_5-Rs (Prilla et al., 2006) are highly effective when interacting with residues of ECL 2 and the ECL 3/TM 7-interface simultaneously. The role of the allosteric site for voltage dependence was underscored by a mutation of $W^{7.35}$, which disrupts allosteric modulation (Prilla et al., 2006). Indeed, the mutation $W^{7.35}$A in Me-R caused a loss in gallamine binding (Figure 7) and the expected uncoupling effect was evident during our voltage-clamp experiments, as M_3-R ($W^{7.35}$A) was entirely insensitive to voltage (F-V curve in Figure 8B). Our MD simulations related this uncoupling effect to a loss of communication between F222 of ECL 2, a key residue for allosteric modulation of the M_3-R (Huang et al., 2005), and the receptor tyrosine lid (Figure 9). The localization of the tyrosines at the interface between the orthosteric site and the allosteric site might also explain why the voltage dependence of ACh-activated receptors was affected by the $W^{7.35}$A mutation. For the M_3-R, $W^{7.35}$ is close to $Y^{7.39}$ and mutation of the tryptophan clearly affected the orientation of $Y^{7.39}$. Our MD simulations point to a differential coupling between residues in ECL 2 and the tyrosine lid through $W^{7.35}$, which was lost in M_3-R ($W^{7.35}$A) (Figure 9). Because these residues in ECL2 are not conserved, there were different $W^{7.35}$/tyrosine lid-interactions in M_1-R compared to M_3-R (Figure 9), which may also explain the different behaviors in response to voltage. These observations open new questions on the mechanistic basis of the observed crosstalk between allosteric and orthosteric muscarinic receptor regions. The simulations presented in this study were run with activated receptor models of the M_2-R structure. Therefore, future studies will greatly benefit from additional structural information on activated M_1-Rs and M_3-Rs to further evaluate the proposed crosstalk mechanism for other M-R subtypes. In addition, the use of simulated electrical fields capable of mimicking membrane depolarizations in the physiological range, as used in our live cell experiments, will help to add more structural details to the molecular mechanism of voltage dependence in M-Rs. This could help to clarify why an exchange of ECL 2 alone was not sufficient to affect voltage sensitivity, but the entire allosteric site was required for a full effect (Figure 5F). Thus, for allostery to occur, ECL 2, ECL 3 and TM 7 require functional coupling. This is compatible with the observation that follow-

ing binding of an AM, the entire allosteric vestibule of M-Rs closes and all three structures are involved in this conformational change (Kruse et al., 2013). Notably, all modifications of allosteric receptor regions of the M_3-R caused a strong reduction in voltage dependence (Figure 5), but never induced an M_1-R response. This indicates that there are additional receptor regions that define the specific response of each M-R subtype to voltage changes. This hypothesis was confirmed by experiments that utilized pilocarpine to activate M-Rs. The M_3-R, but also M_3-BQCA-R and M_3-R ($W^{7.35}A$), which were both insensitive to voltage in the ACh-activated conformation, displayed a clearly detectable voltage dependence with an opposite polarity (Figure 10 B through D). This pilocarpine-effect on the voltage dependence has been described before for M_2-Rs (Navarro-Polanco et al., 2011; Moreno-Galindo et al., 2016) and M_3-Rs (Rinne et al., 2015). The observed turn from deactivation (ACh/M_3-R) into activation (pilocarpine/M_3R) during membrane depolarization was attributed to different ligand interaction patterns (Rinne et al., 2015), which may induce different populations of active receptor conformations. One molecular element that discerns both binding modes and linked them to differences in receptor activation was a well pronounced (ACh) or weak (pilocarpine) interaction with TM 6, which is crucial for M-R activation (Kruse et al., 2012). These findings imply the following things: (*i*) The allosteric site controls voltage sensitivity and receptor signaling in M-Rs by direct communication with the orthosteric tyrosine lid. It may not contain a voltage sensing structure. This novel route of communication between the allosteric site, the tyrosine lid, ACh and the orthosteric site may explain the observed different voltage dependencies of M_1-Rs and M_3-Rs. The probe dependency of the voltage effect between ACh and pilocarpine allows us to speculate that the unique binding mode of pilocarpine may not require the same degree of interaction with the tyrosine lid. (*ii*) It appears that additional residues of the orthosteric site and elsewhere may contribute to voltage sensitivity in M-Rs. Putative voltage sensing structures in M-Rs are discussed below. (iii) Modulation of M-Rs by voltage shares important properties of allostery. However, additional studies will be required to reveal whether the precise intramolecular pathways for both types of modulations are coincident in M-Rs.

4.2 Voltage sensors in GPCRs

Recently, two alternative voltage sensors have been described for class A GPCRs: The first sensor is an "internal" sodium ion that has been detected in several crystal structures of inactive class A GPCRs. The Na^+ ion binds to a conserved aspartate of TM 2 ($D^{2.50}$) below the orthosteric site and stabilizes the inactive receptor conformation (Liu et al., 2012). Conversely, in receptors with an orthosteric agonist bound, the Na^+ binding pocket collapses as Na^+ is released from $D^{2.50}$ during receptor activation (Gutiérrez-de-Terán et al., 2013; Katritch et al., 2014; Massink et al., 2015; Miao et al., 2015). A Na^+ ion represents the ideal voltage sensor: It carries a charge of +1, which is in agreement with previously reported charges in GPCRs that move during depolarization (Ben-Chaim et al., 2006; Navarro-Polanco et al., 2011; Rinne et al., 2013; Birk et al., 2015; Rinne et al., 2015), and its binding site is exposed to the electrical field across the membrane. A depolarization of the membrane would then cause the release of the Na^+ ion from $D^{2.50}$, inducing a change in receptor conformation. However, even though this mechanism has been analyzed and observed in MD-simulations of inactive states of M_2-Rs and δ-Opioid-Rs (Vickery et al., 2016), experimental data from live cell experiments are less conclusive: While mutations of $D^{2.50}$ eliminated gating currents in M_2-Rs (shown for $D^{2.50}A$) (Navarro-Polanco et al., 2011), voltage sensitivities for agonist binding and conformational changes of the receptor were still present (shown for $D^{2.50}N$) (Barchad-Avitzur et al., 2016). This is in line with our experimental obervations and confirms the presence of multiple voltage sensing receptor structures in M-Rs (see below).

Another study has identified the tyrosine lid of the orthosteric binding site as an alternative voltage sensor for the M_2-R (Barchad-Avitzur et al., 2016). The voltage sensitivity was attributed to dipole moments of the tyrosine residues and gating currents were clearly affected by mutations that neutralized the dipoles. Again, the single mutations $Y^{3.33}A$ or $Y^{3.33}F$, which had the strongest effect on repressing gating currents, did not fully eliminate the voltage dependence of agonist binding or voltage sensitive changes in receptor conformation (Barchad-Avitzur et al., 2016). As shown in Figure 10A, a neutralization of all three tyrosines also failed to abolish the voltage dependence in M_3-Rs. Instead, the ACh/mutant receptor complex was voltage sensitive and displayed activation in response to depolarization. One of the key el-

ements for the activation of M-Rs is the flexibility of TM 6 (Kruse et al., 2013). In the light of the pilocarpine results described above, the observed activation of ACh-bound M_3-R (FFF) by voltage can be interpreted as follows: Mutations of the tyrosine lid may influence the architecture of the orthosteric site, causing ACh to bind in a "pilocarpine-like" mode (see (Rinne et al., 2015) and the ligand may directly affect the position or flexibility of TM 6. Alternatively, because $Y^{6.51}$ contributes to the lid structure, it seems plausible that the assembly of all three tyrosine residues may directly affect the orientation and/or flexibility of TM 6. These properties are altered in the mutant receptor. Consequently, M_3-R (FFF) switches to a different conformation than wild type M_3-R before and during depolarization. This interpretation may also explain why our allosteric chimeras, which may have a more indirect effect on the conformation of the tyrosine lid (Figure 9), displayed only an intermediate phenotype in response to voltage (Figures 5 and 6). In conclusion, our results with M-R constructs that carry a non-functional tyrosine lid uncover independent receptor regions that also contribute to voltage effects.

5. Conclusion and implications for the future

Our study has identified an intramolecular pathway for the modulation of M-R function by voltage, which involves a direct communication between structures of the orthosteric site with the allosteric site. Our MD simulations provide evidence that this crosstalk between both sites is different in M_1-Rs and M_3-Rs, which may explain previously observed receptor subtype- and agonist-specific responses to voltage. One of the major findings is that regulation of M-R function by the membrane potential shares features of allosteric modulation, such as probe dependency, and can therefore be regarded as an additional type of AM for receptor function. There is increasing experimental evidence that this type of receptor regulation occurs under physiological conditions. Biophysical properties of M_1-Rs (Ben-Chaim et al., 2006), M_2-Rs (Navarro-Polanco et al., 2011) and M_3-Rs (Rinne et al., 2015) lead to V_{50} values that lie in a range between - 70 mV and -40 mV, which is compatible with physiological V_M changes and in agreement with our data (Figure 8). One may be concerned about the fact that some M-Rs, such as the M_1-R that is expressed in neurons, are rather exposed to short trains of action potentials than to long lasting

depolarizations. However, the M_1-R also responded to "neuronal stimulation patterns" and showed an increase in activation at higher depolarization frequencies (Figure S4). This positive modulation of GPCRs by V_M may sensitize receptor signaling at given agonist concentrations and has been shown to control IP_3-mediated Ca^{2+} release (Gurung et al., 2008; Rinne et al., 2015). Furthermore, the voltage dependence of endogenous M_2-Rs controls neurotransmitter release at synapses (Kupchik et al., 2011) or shapes GIRK channel currents in adult cardiac myocytes (Navarro-Polanco et al., 2013). Of note, some of the synthetic receptor constructs identified in this study, which are insensitive to voltage but bind ACh with high affinity (Figure S1), may be useful for future animal studies to identify more signaling pathways that are regulated by the voltage-sensitivity of these receptors.

Declaration of interest

The authors declare no conflicts of interest in this work.

Funding sources

This work was supported by the Deutsche Forschungsgemeinschaft (DFG): SFB 539, TPA 13 to M.B; Emmy-Noether fellowship KO-4095/1-1, Heisenberg professorship KO-4095/4-1 and individual grant KO-4095/3-1 to P.K and Ri 1908/2-1 to A.R. The authors M.M-S., M.B. and P.K. participated in European Cooperation for Science and Technology (COST) Action CM1207 "GLISTEN". A.R. was supported by Forschungsförderung Ruhruniversität Medizin (FoRUM, F809-2014).

Author contributions

M.M.-S, P.K. and A.R. participated in research design. M.B. and P.K. provided analytical tools and reagents. A.H., A.R., M.D. and M.M.-S. conducted experiments and performed data analysis. M.M.-S., P.K., M.B. and A.R. wrote the manuscript.

Acknowledgements

The authors would like to thank Anke Galhoff for excellent technical support.

References

Abdul-Ridha A, Lane JR, Mistry SN, Lopez L, Sexton PM, Scammells PJ, Christopoulos A, and Canals M (2014a) Mechanistic insights into allosteric structure-function relationships at the M1 muscarinic acetylcholine receptor. *J Biol Chem* **289:**33701–33711 doi: 10.1074/jbc.M114.604967.

Abdul-Ridha A, López L, Keov P, Thal DM, Mistry SN, Sexton PM, Lane JR, Canals M, and Christopoulos A (2014b) Molecular determinants of allosteric modulation at the M1 muscarinic acetylcholine receptor. *J. Biol. Chem.* **289:**6067–6079 doi: 10.1074/jbc.M113.539080.

Barchad-Avitzur O, Priest MF, Dekel N, Bezanilla F, Parnas H, and Ben-Chaim Y (2016) A Novel Voltage Sensor in the Orthosteric Binding Site of the M2 Muscarinic Receptor. *Biophys. J.* **111:**1396–1408 doi: 10.1016/j.bpj.2016.08.035.

Ben-Chaim Y, Chanda B, Dascal N, Bezanilla F, Parnas I, and Parnas H (2006) Movement of 'gating charge' is coupled to ligand binding in a G-protein-coupled receptor. *Nature* **444:**106–109 doi: 10.1038/nature05259.

Ben-Chaim Y, Tour O, Dascal N, Parnas I, and Parnas H (2003) The M2 muscarinic G-protein-coupled receptor is voltage-sensitive. *The Journal of biological chemistry* **278:**22482–22491 doi: 10.1074/jbc.M301146200.

Birk A, Rinne A, and Bunemann M (2015) Membrane Potential Controls the Efficacy of Catecholamine-induced beta1-Adrenoceptor Activity. *J Biol Chem* **290:**27311–27320 doi: 10.1074/jbc.M115.665000.

Bock A, Merten N, Schrage R, Dallanoce C, Bätz J, Klöckner J, Schmitz J, Matera C, Simon K, Kebig A, Peters L, Müller A, Schrobang-Ley J, Tränkle C, Hoffmann C, Amici M de, Holzgrabe U, Kostenis E, and Mohr K (2012) The allosteric vestibule of a seven transmembrane helical receptor controls G-protein coupling. *Nat Commun* **3:**1044 doi: 10.1038/ncomms2028.

Conn PJ, Christopoulos A, and Lindsley CW (2009) Allosteric modulators of GPCRs: a novel approach for the treatment of CNS disorders. *Nature reviews. Drug discovery* **8:**41–54 doi: 10.1038/nrd2760.

Ehlert FJ and Griffin MT (2008) Two-state models and the analysis of the allosteric effect of gallamine at the M2 muscarinic receptor. *The Journal of pharmacology and experimental therapeutics* **325:**1039–1060 doi: 10.1124/jpet.108.136960.

Gnagey AL, Seidenberg M, and Ellis J (1999) Site-Directed Mutagenesis Reveals Two Epitopes Involved in the Subtype Selectivity of the Allosteric Interactions of Gallamine at Muscarinic Acetylcholine Receptors. *Mol Pharmacol* **56:**1245–1253 doi: 10.1124/mol.56.6.1245.

Gurung IS, Martinez-Pinna J, and Mahaut-Smith MP (2008) Novel consequences of voltage-dependence to G-protein-coupled P2Y1 receptors. *British journal of pharmacology* **154:**882–889 doi: 10.1038/bjp.2008.97.

Gutiérrez-de-Terán H, Massink A, Rodríguez D, Liu W, Han GW, Joseph JS, Katritch I, Heitman LH, Xia L, IJzerman AP, Cherezov V, Katritch V, and Stevens RC (2013) The Role of a Sodium Ion Binding Site in the Allosteric Modulation of the A2A Adenosine G Protein-Coupled Receptor. *Structure* **21:**2175–2185 doi: 10.1016/j.str.2013.09.020.

Harvey MJ, Giupponi G, and Fabritiis GD (2009) ACEMD: Accelerating Biomolecular Dynamics in the Microsecond Time Scale. *J Chem Theory Comput* **5:**1632–1639 doi: 10.1021/ct9000685.

Hoffmann C, Nuber S, Zabel U, Ziegler N, Winkler C, Hein P, Berlot CH, Bunemann M, and Lohse MJ (2012) Comparison of the activation kinetics of the M3 acetylcholine receptor and a constitutively active mutant receptor in living cells. *Molecular pharmacology* **82:**236–245 doi: 10.1124/mol.112.077578.

Huang X-P, Prilla S, Mohr K, and Ellis J (2005) Critical amino acid residues of the common allosteric site on the M2 muscarinic acetylcholine receptor: more similarities than differences between the structurally divergent agents gallamine and bis(ammonio)alkane-type hexamethylene-bis-dimethyl-(3-phthalimidopropyl)ammoniumdibromide. *Mol Pharmacol* **68:**769–778 doi: 10.1124/mol.105.014043.

Katritch V, Fenalti G, Abola EE, Roth BL, Cherezov V, and Stevens RC (2014) Allosteric sodium in class A GPCR signaling. *Trends Biochem. Sci.* **39:**233–244 doi: 10.1016/j.tibs.2014.03.002.

Kruse AC, Hu J, Pan AC, Arlow DH, Rosenbaum DM, Rosemond E, Green HF, Liu T, Chae PS, Dror RO, Shaw DE, Weis WI, Wess J, and Kobilka BK (2012) Structure and dynamics of the M3 muscarinic acetylcholine receptor. *Nature* **482:**552–556 doi: 10.1038/nature10867.

Kruse AC, Ring AM, Manglik A, Hu J, Hu K, Eitel K, Hübner H, Pardon E, Valant C, Sexton PM, Christopoulos A, Felder CC, Gmeiner P, Steyaert J, Weis WI, Garcia KC, Wess J, and Kobilka BK (2013) Activation and allosteric modulation of a muscarinic acetylcholine receptor. *Nature* **504:**101–106 doi: 10.1038/nature12735.

Kupchik YM, Barchad-Avitzur O, Wess J, Ben-Chaim Y, Parnas I, and Parnas H (2011) A novel fast mechanism for GPCR-mediated signal transduction--control of neurotransmitter release. *J Cell Biol* **192:**137–151 doi: 10.1083/jcb.201007053.

Li H, Robertson AD, and Jensen JH (2005) Very fast empirical prediction and rationalization of protein pKa values. *Proteins* **61:**704–721 doi: 10.1002/prot.20660.

Liu W, Chun E, Thompson AA, Chubukov P, Xu F, Katritch V, Han GW, Roth CB, Heitman LH, IJzerman AP, Cherezov V, and Stevens RC (2012) Structural basis for allosteric regulation of GPCRs by sodium ions. *Science* **337:**232–236 doi: 10.1126/science.1219218.

Ma L, Seager MA, Wittmann M, Jacobson M, Bickel D, Burno M, Jones K, Graufelds VK, Xu G, Pearson M, McCampbell A, Gaspar R, Shughrue P, Danziger A, Regan C, Flick R, Pascarella D, Garson S, Doran S, Kreatsoulas C, Veng L, Lindsley CW, Shipe W, Kuduk S, Sur C, Kinney G, Seabrook GR, and Ray WJ (2009) Selective activation of the M1 muscarinic acetylcholine receptor achieved by allosteric potentiation. *Proceedings of the National Academy of Sciences* **106:**15950–15955 doi: 10.1073/pnas.0900903106.

Massink A, Gutierrez-de-Teran H, Lenselink EB, Ortiz Zacarias NV, Xia L, Heitman LH, Katritch V, Stevens RC, and IJzerman AP (2015) Sodium ion binding pocket mutations and adenosine A2A receptor function. *Mol Pharmacol* **87:**305–313 doi: 10.1124/mol.114.095737.

Miao Y, Caliman AD, and McCammon JA (2015) Allosteric effects of sodium ion binding on activation of the m3 muscarinic g-protein-coupled receptor. *Biophys. J.* **108:**1796–1806 doi: 10.1016/j.bpj.2015.03.003.

Moreno-Galindo EG, Alamilla J, Sanchez-Chapula JA, Tristani-Firouzi M, and Navarro-Polanco RA (2016) The agonist-specific voltage dependence of M2 muscarinic receptors modulates the deactivation of the acetylcholine-gated K current (I). *Pflugers Arch* doi: 10.1007/s00424-016-1812-y.

Navarro-Polanco RA, Arechiga-Figueroa IA, Salazar-Fajardo PD, Benavides-Haro DE, Rodriguez-Elias JC, Sachse FB, Tristani-Firouzi M, Sanchez-Chapula JA, and Moreno-Galindo EG (2013) Voltage sensitivity of M2 muscarinic receptors underlies the delayed rectifier-like activation of ACh-gated K+ current (IKACh) by choline in feline atrial myocytes. *The Journal of physiology* doi: 10.1113/jphysiol.2013.255166.

Navarro-Polanco RA, Moreno Galindo, E. G., Ferrer-Villada T, Arias M, Rigby JR, Sanchez-Chapula JA, and Tristani-Firouzi M (2011) Conformational changes in the M2 muscarinic receptor induced by membrane voltage and agonist binding. *The Journal of physiology* **589:**1741–1753 doi: 10.1113/jphysiol.2010.204107.

Prilla S, Schrobang J, Ellis J, Holtje H-D, and Mohr K (2006) Allosteric interactions with muscarinic acetylcholine receptors: complex role of the conserved tryptophan M2422Trp in a critical cluster of amino acids for baseline affinity, subtype selectivity, and cooperativity. *Mol Pharmacol* **70:**181–193 doi: 10.1124/mol.106.023481.

Rinne A, Birk A, and Bunemann M (2013) Voltage regulates adrenergic receptor function. *Proceedings of the National Academy of Sciences of the United States of America* **110:**1536–1541 doi: 10.1073/pnas.1212656110.

Rinne A, Mobarec JC, Mahaut-Smith M, Kolb P, and Bunemann M (2015) The mode of agonist binding to a G protein-coupled receptor switches the effect that voltage changes have on signaling. *Sci Signal* **8:**ra110 doi: 10.1126/scisignal.aac7419.

Shirey JK, Brady AE, Jones PJ, Davis AA, Bridges TM, Kennedy JP, Jadhav SB, Menon UN, Xiang Z, Watson ML, Christian EP, Doherty JJ, Quirk MC, Snyder DH, Lah JJ, Levey AI, Nicolle MM, Lindsley CW, and Conn PJ (2009) A selective allosteric potentiator of the M1 muscarinic acetylcholine receptor increases activity of medial prefrontal cortical neurons and restores impairments in reversal learning. *J Neurosci* **29:**14271–14286 doi: 10.1523/JNEUROSCI.3930-09.2009.

Shivnaraine RV, Kelly B, Sankar KS, Redka D'yS, Han YR, Huang F, Elmslie G, Pinto D, Li Y, Rocheleau JV, Gradinaru CC, Ellis J, and Wells JW (2016) Allosteric modulation in monomers and oligomers of a G protein-coupled receptor. *Elife* **5** doi: 10.7554/eLife.11685.

Thal DM, Sun B, Feng D, Nawaratne V, Leach K, Felder CC, Bures MG, Evans DA, Weis WI, Bachhawat P, Kobilka TS, Sexton PM, Kobilka BK, and Christopoulos A (2016) Crystal structures of the M1 and M4 muscarinic acetylcholine receptors. *Nature* **531:**335–340 doi: 10.1038/nature17188.

Vickery ON, MacHtens J-P, Tamburrino G, Seeliger D, and Zachariae U (2016) Structural Mechanisms of Voltage Sensing in G Protein-Coupled Receptors. *Structure:*1–11 doi: 10.1016/j.str.2016.04.007.

Wootten D, Christopoulos A, and Sexton PM (2013) Emerging paradigms in GPCR allostery: implications for drug discovery. *Nature reviews. Drug discovery* **12:**630–644 doi: 10.1038/nrd4052.

Wu EL, Cheng X, Jo S, Rui H, Song KC, Davila-Contreras EM, Qi Y, Lee J, Monje-Galvan V, Venable RM, Klauda JB, and Im W (2014) CHARMM-GUI Membrane Builder toward realistic biological membrane simulations. *J Comput Chem* **35:**1997–2004 doi: 10.1002/jcc.23702.

Figure Captions

Figure 1: Modulation of M-R function by voltage or by allosteric modulators. A: Application of ACh to single HEK 293 cells expressing M_1-R and the G_q biosensor caused a reduction in the FRET ratio (F_{YFP}/F_{CFP}), reflecting activation of M_1-R and G_q. A depolarization of the membrane from -90 mV to +40 mV resulted in a further decrease in FRET (upper panel, n = 5). Lower panel: Depolarization in the absence of ACh had no effect on receptor signaling (n = 8). B: Co-application of the positive allosteric modulator BQCA and 20 nM ACh to cells expressing M_1-R and the G_q biosensor caused a further decrease in FRET (upper panel, n = 10). Lower panel: Application of BQCA alone had no effect on receptor signaling (n = 6). C: Application of ACh to cells expressing M_3-R caused activation of G_q at -90 mV, but the voltage step caused deactivation of G_q and M_3-R at +40 mV (upper panel, n = 6) Lower panel: Depolarization in the absence of ACh had no effect on receptor signaling (n = 8). D: Application of the negative allosteric modulator Gallamine to cells expressing M_3-R inhibited G_q signaling in the presence of ACh (n = 8). Lower panel: The application of Gallamine alone did not change receptor signaling (n = 6). Data are presented as mean (black) ± sem (grey).

Figure 2: Voltage dependence of the M_1-R in the presence of BQCA. BQCA did not affect the voltage dependence of M_1-R at moderate (500 nM, A) or higher concentrations (B, 2 µM, n = 5). Data are presented as mean (black) ± sem (grey).

Figure 3: **Pharmacology of the allosteric chimera M_3-BQCA-R** A: Cartoon of the M_1-R (red, left panel). The positive allosteric modulator BQCA facilitated receptor signaling of M_1-R in the presence of 10 nM ACh (n = 10) to reach full activation of G_q (reference: 100 µM ACh, right panel)) B: Cartoon of M_3-R (grey, left panel). This receptor subtype was insensitive to the same concentrations of BQCA in the presence of ACh (n = 7). C: Cartoon of the chimera M_3-BQCA-R (left panel). M_3-BQCA-R acquired sensitiv-

ity to BQCA, which potentiated the activation of G_q in the presence of ACh (50 nM) in a concentration-dependent manner (n = 6). Data are presented as mean (black) ± sem (grey).

Figure 4: Pharmacology of other allosteric M_3-R/M_1-R chimeras. Chimeras were based on M_3-R (cartoon: grey) and contained selected fragments of the M_1-R allosteric site (cartoon: red). A: An M_3-R with ECL 2 from M_1-R did not respond to BQCA (n = 9). B: Incorporation of ECL 3 and TM 7 resulted in a BQCA-sensitive M_3-R (n = 8). C: The transfer of TM 7 alone did not mediate BQCA-selectivity (n = 7). D: The transfer of ECL 2 and ECL3 resulted in BQCA-selectivity (n = 5). Data are presented as mean (black) ± sem (grey).

Figure 5: Voltage dependence of M_3-R/M_1-R chimeras. A: The chimera M_3-BQCA-R was almost insensitive to depolarization in the presence of ACh (n = 7). B: Substitution of extracellular loop 2 (ECL 2) alone had no affect on the voltage dependence of M_3-R (n = 7). C: Substitutions of ECL 2 and ECL 3 caused a mild reduction in voltage dependence (n = 7). D: Replacing ECL 3 and TM 7 caused a stronger reduction in voltage dependence (n = 5). E: The single substitution of TM 7 had only a modest effect on the voltage dependence (n = 6). The nominal concentrations of ACh represent the EC_{50}-values for each construct (Supplemental Figure 2). The dashed line indicates the magnitude of deactivation by voltage for the parental M_3-R (EC_{50}: 20 nM ACh, data from Figure 1C). F: Statistical analysis of the inhibitory effect that depolarization had on various M_3-R chimeras at their given EC_{50}-values for ACh. The columns highlighted in grey represent chimeras that acquired sensitivity to BQCA (see Figure 3). ** denotes $p < 0.01$, *** denotes $p < 0.001$, n.s.: not significant. Data are presented as mean ± sem of n individual cells. In the cartoons M_3-R is depicted in grey and fragments of M_1-R are depicted in red.

Figure 6: Voltage dependence of a M_1/M_3-R chimera. A: Cartoon of a M_1/M_3-R chimera consisting of TM 1-4 of M_1-R (grey) and TM 5-7 of M_3-R (red). B: Application of 10 nM ACh to cells expressing the chimera and the G_q biosensor resulted in activation of the chimera. Co-application of gallamine caused deactivation of the chimera (n = 10). C: Summarized data comparing the extend of deactivation by 100

μM gallamine at the level of 50 % receptor activation (EC_{50}-values for ACh are given in Figure 10). D: The chimera was insensitive to a depolarization of the membrane (n = 6). Data are presented as mean (black) ± sem (grey). * denotes $p < 0.05$, n.s.: not significant.

Figure 7: **The mutation $W^{7.35}A$ eliminated the voltage dependence of ACh-activated M_3-R.** A: The mutant receptor M_3-R ($W^{7.35}A$) responded to an application of ACh with G_q-activation, but was almost insensitive to gallamine (n = 8). The dashed line represents the response of wild type M_3-R to the same concentration of gallamine (mean value from Figure 1D). B: The mutant receptor did not show any detectable voltage sensitivity (n = 7). The dashed line represents the response of wild type M_3-R to the same voltage step (mean value taken from Figure 1C). Data are presented as mean (black) ± sem (grey).

Figure 8: F-V curves of M_1-R, M_3-R, M_3-BQCA-R and M_3-R (W7.35A). A: The F-V curve of the M_1-R showed a sigmoidal shape and activation at positive membrane potentials. B: The M_3R displayed voltage sensitivity in the shape of a sigmoidal F-V curve with decreasing activity at positive membrane potentials. The z-values derived from these curves were 1.07 for the M_1-R and 0.65 for the M_3-R. The potential V_{50} refers to the value of V_M at 50 % receptor activation and was calculated as -51 mV for the M_1-R and -42 mV for the M_3-R. In contrast to the parental receptor, the F-V curve of the M_1/M_3-R chimera was linear with no detectable voltage sensitivity (A). The chimera M_3-BQCA-R displayed a strongly reduced voltage sensitivity with a V_{50}-value that was shifted to -84 mV. The allosteric receptor mutant M_3-R ($W^{7.35}A$) was voltage insensitive (linear F-V relationship). n = 5 to 14 cells per data point. Data are presented as mean ± sem.

Figure 9: Molecular dynamics (MD) simulations of active muscarinic receptor structures. A: Cartoon representation of an active receptor model with the analyzed receptor region connecting the extracellular allosteric site and the tyrosine lid, highlighted as a grey box. The tyrosine lid belongs to the orthosteric ACh-binding site and contains $Y^{3.33}$, $Y^{6.51}$ and $Y^{7.39}$. B through E: Different conformations of the residues of interest can be observed for the M_1-R (B), the M_3-R (C), the M_3-BQCA-R (D) and M_3-R ($W^{7.35}A$) (E). Receptor regions from the M_1-R are coloured in red, regions from the M_3-R are depicted in

white. Two alternative conformations of the residues of interest are shown per receptor. Part of the ECL 2 is shown as cartoon and the ACh binding site is depicted in lime in CPK representation for reference. See text for further details on MD simulations.

Figure 10: Voltage dependence of a tyrosine lid mutant and pilocarpine-activated M_3-Rs. A: A mutant M_3-R, in which the three tyrosines of the tyrosine lid structure were replaced with phenylalanine, was voltage sensitive and activated by depolarization (n = 10). B: Wild type M_3-R was activated by depolarization in the presence of the partial agonist pilocarpine (n = 8). C, D: The pilocarpine-activated receptor mutant M_3-R ($W^{7.35}A$) (n = 5) and the chimera M_3-BQCA-R (n = 9) displayed a clearly detectable voltage sensitivity. The nominal concentrations of ACh and pilocarpine reflect the corresponding EC_{50}-values for each construct. Data are presented as mean (black) ± sem (grey).

Figures

Figure 1

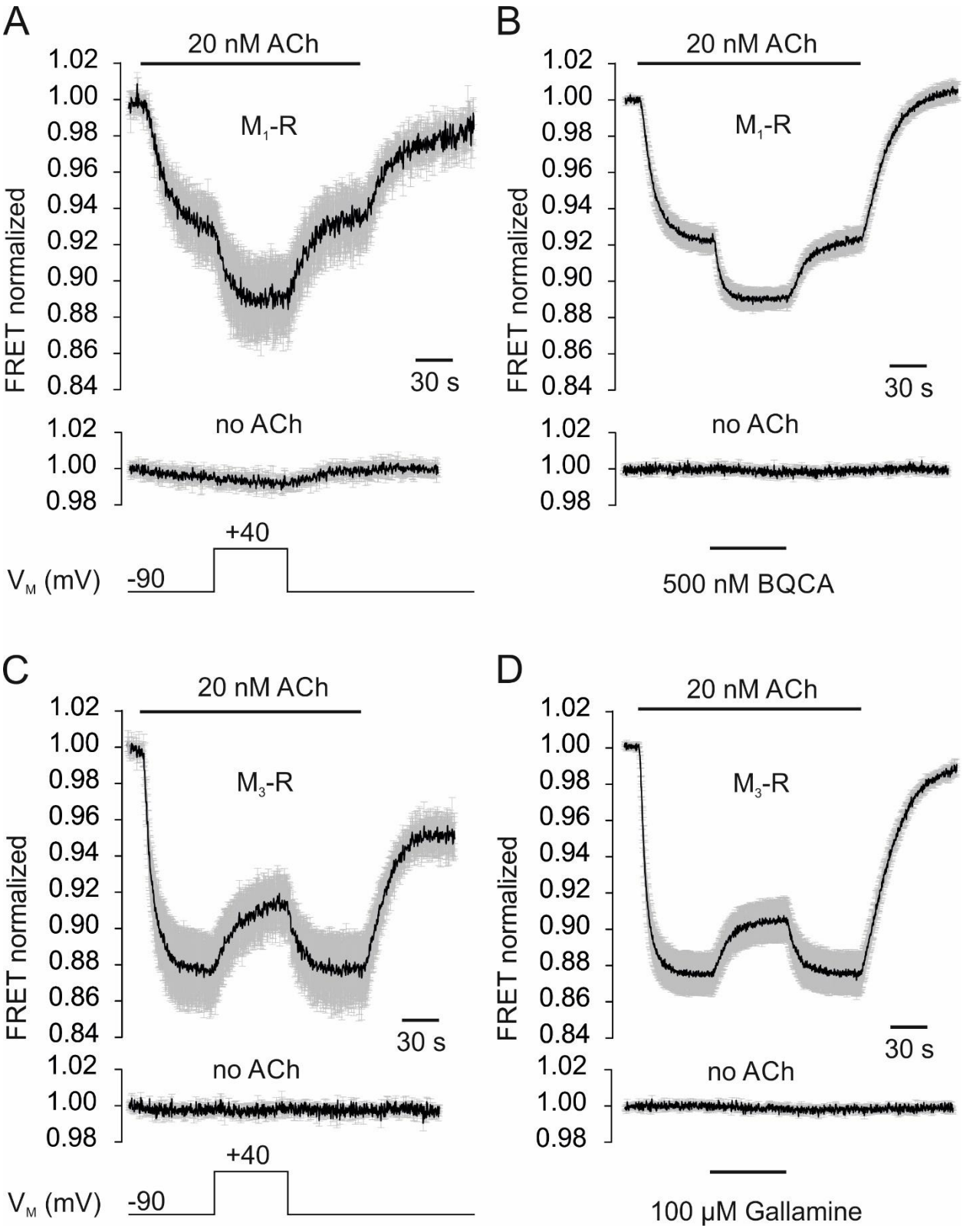

Figure 2

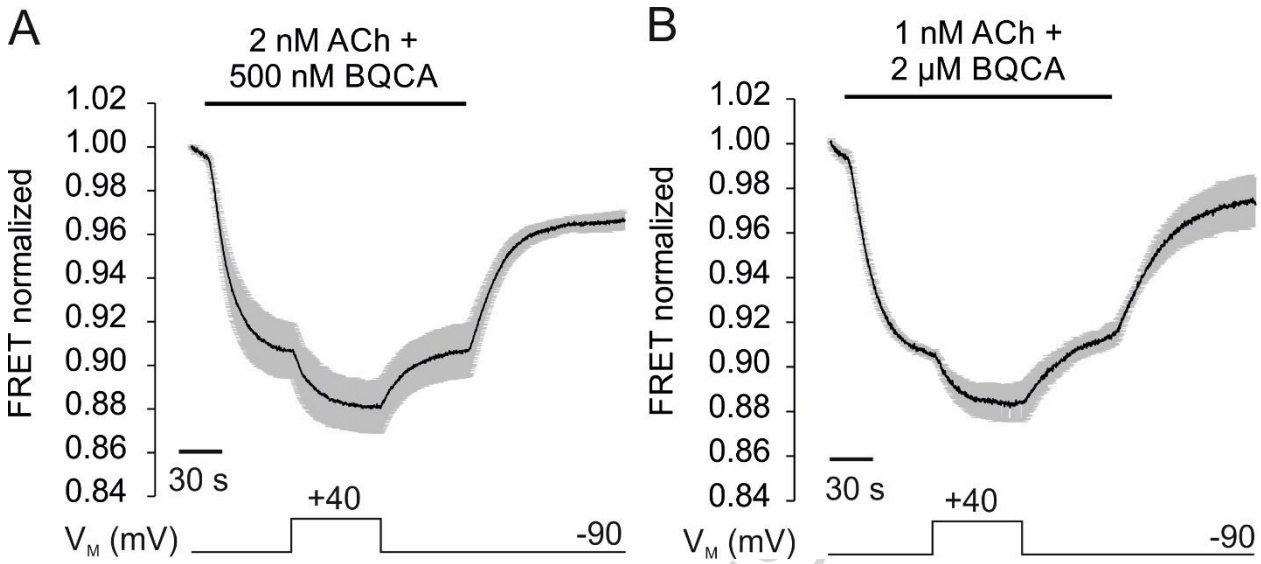

Figure 3

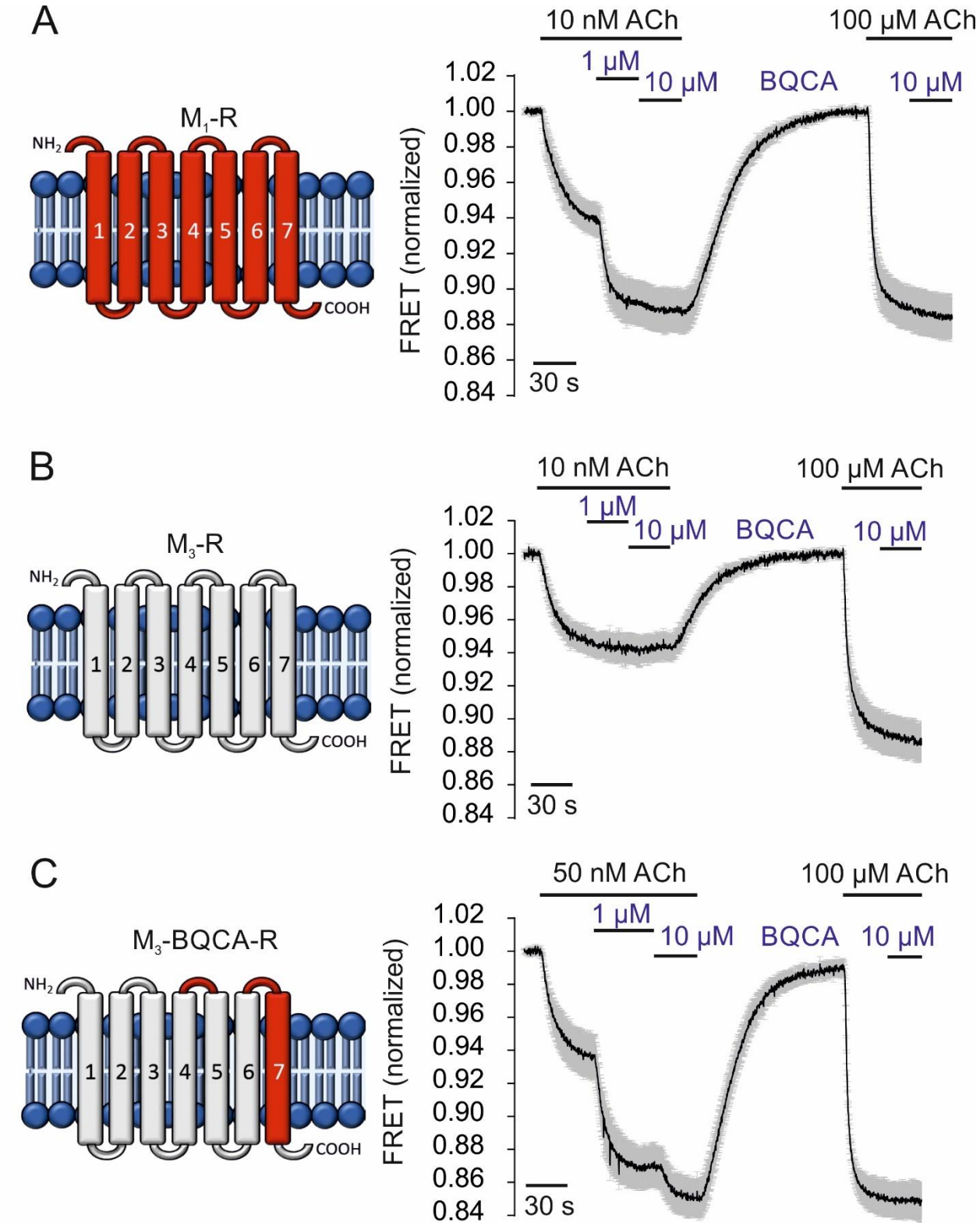
A
M1-R
NH2
1 2 3 4 5 6 7
COOH
10 nM ACh
100 µM ACh
1 µM
10 µM
BQCA
10 µM
FRET (normalized)
1.02
1.00
0.98
0.96
0.94
0.92
0.90
0.88
0.86
0.84
30 s
B
M3-R
NH2
1 2 3 4 5 6 7
COOH
10 nM ACh
100 µM ACh
1 µM
10 µM
BQCA
10 µM
FRET (normalized)
30 s
C
M3-BQCA-R
NH2
1 2 3 4 5 6 7
COOH
50 nM ACh
100 µM ACh
1 µM
10 µM
BQCA
10 µM
FRET (normalized)
30 s

Figure 4

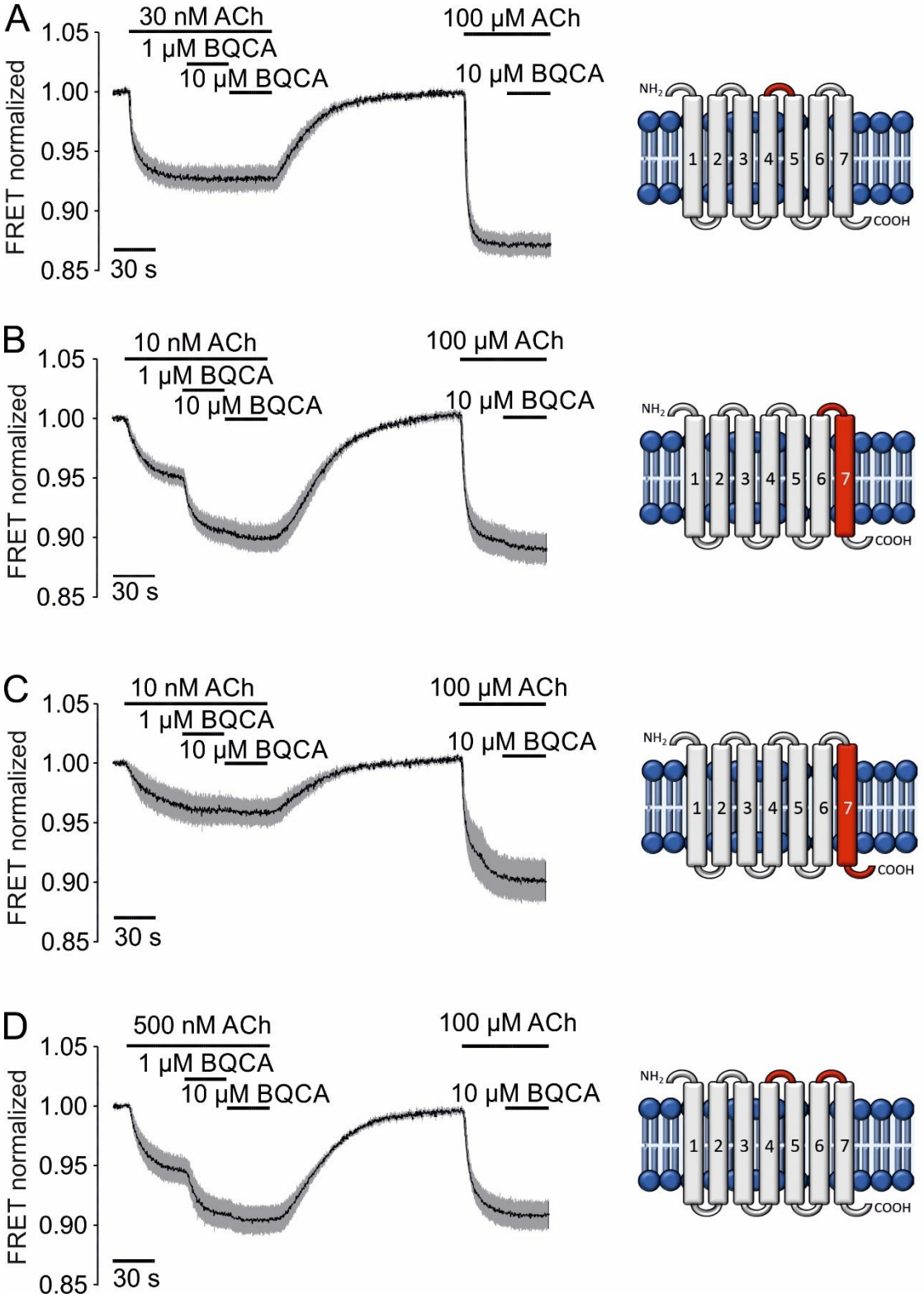

Figure 5

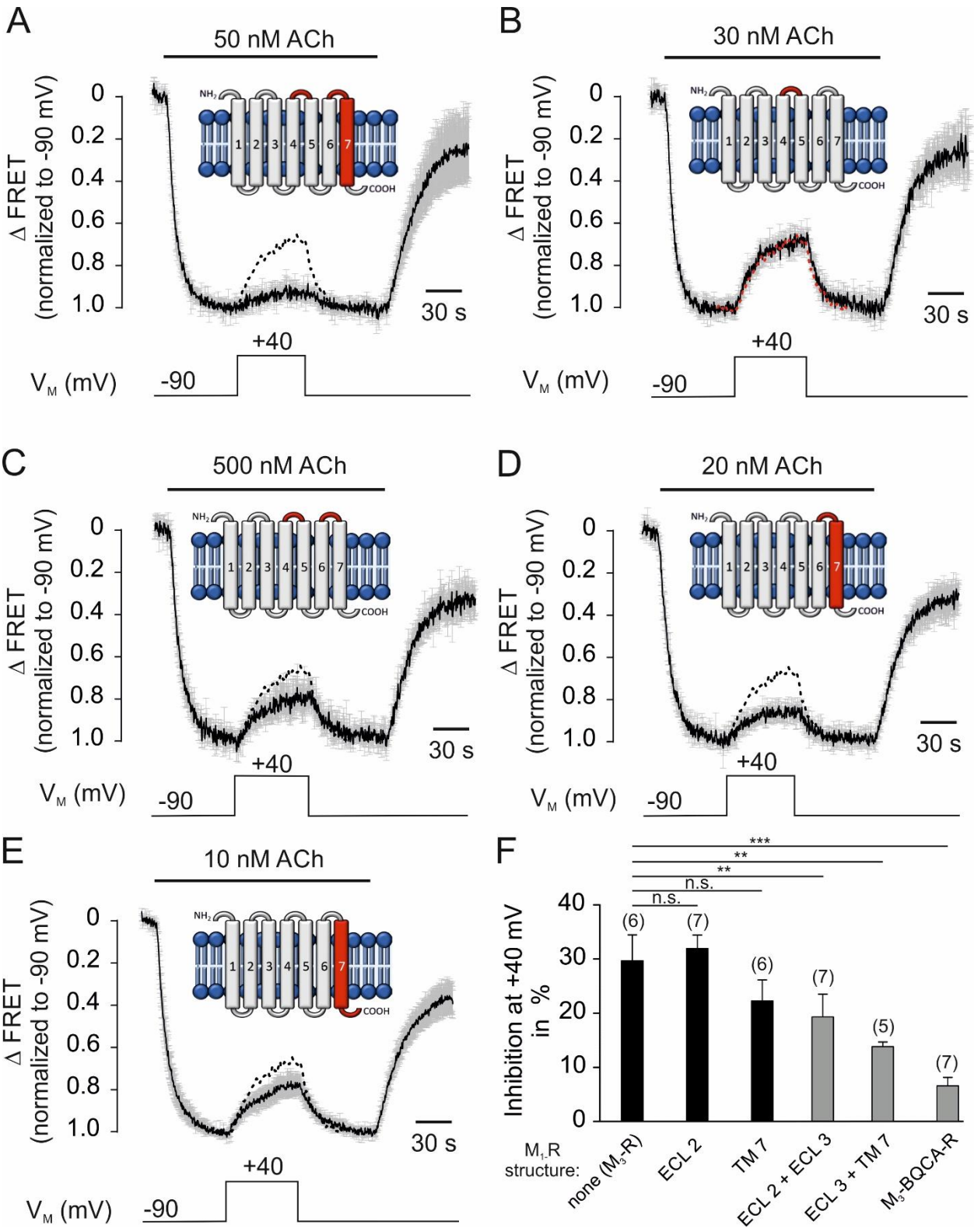
A
50 nM ACh
B
30 nM ACh
C
500 nM ACh
D
20 nM ACh
E
10 nM ACh
F
Δ FRET (normalized to -90 mV)
0
0.2
0.4
0.6
0.8
1.0
30 s
+40
-90
V_M (mV)
NH2
COOH
1 2 3 4 5 6 7
Inhibition at +40 mV in %
40
30
20
10
0
(6)
(7)
(6)
(7)
(5)
(7)
***
**
**
n.s.
n.s.
M1-R structure:
none (M3-R)
ECL 2
TM 7
ECL 2 + ECL 3
ECL 3 + TM 7
M3-BQCA-R

Figure 6

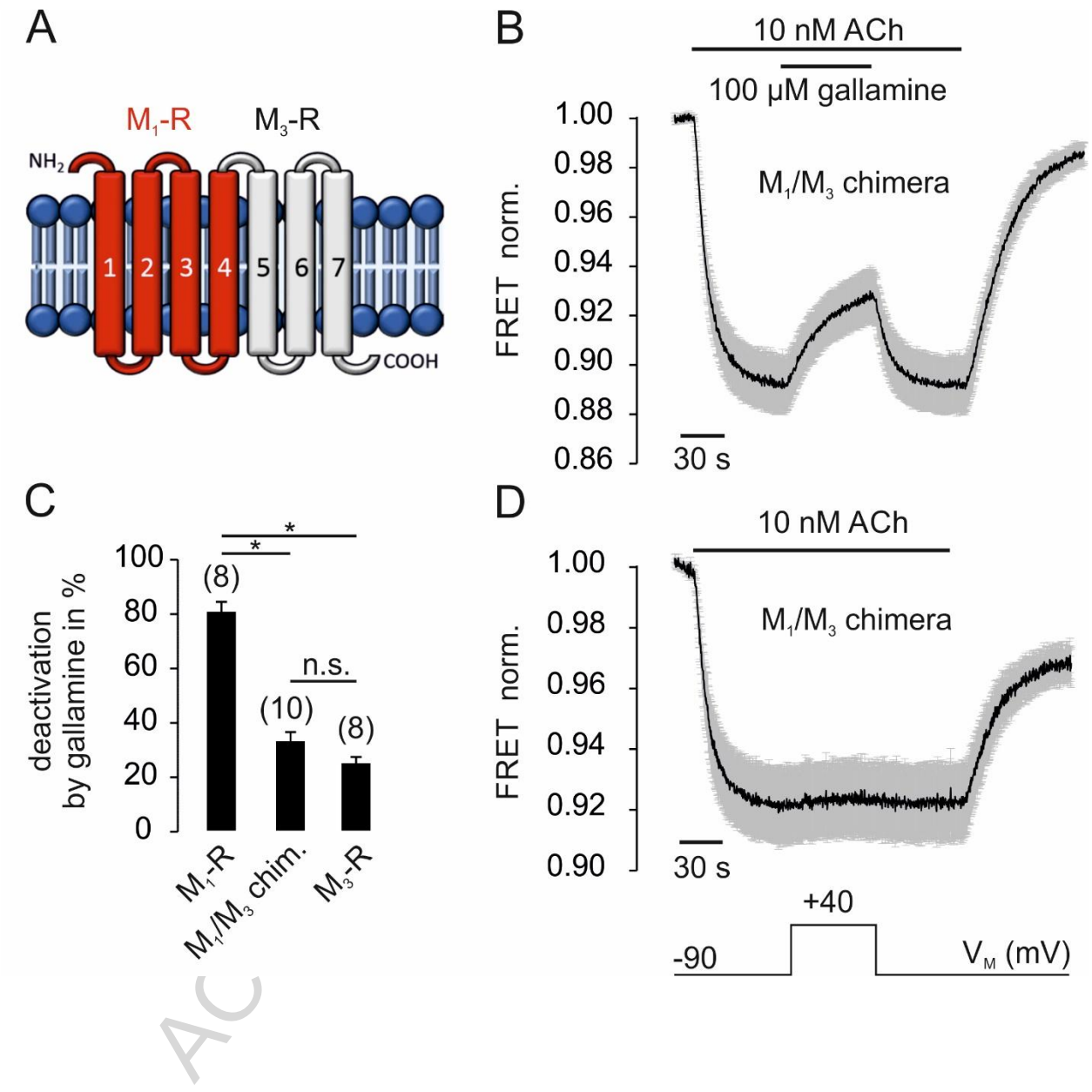

Figure 7

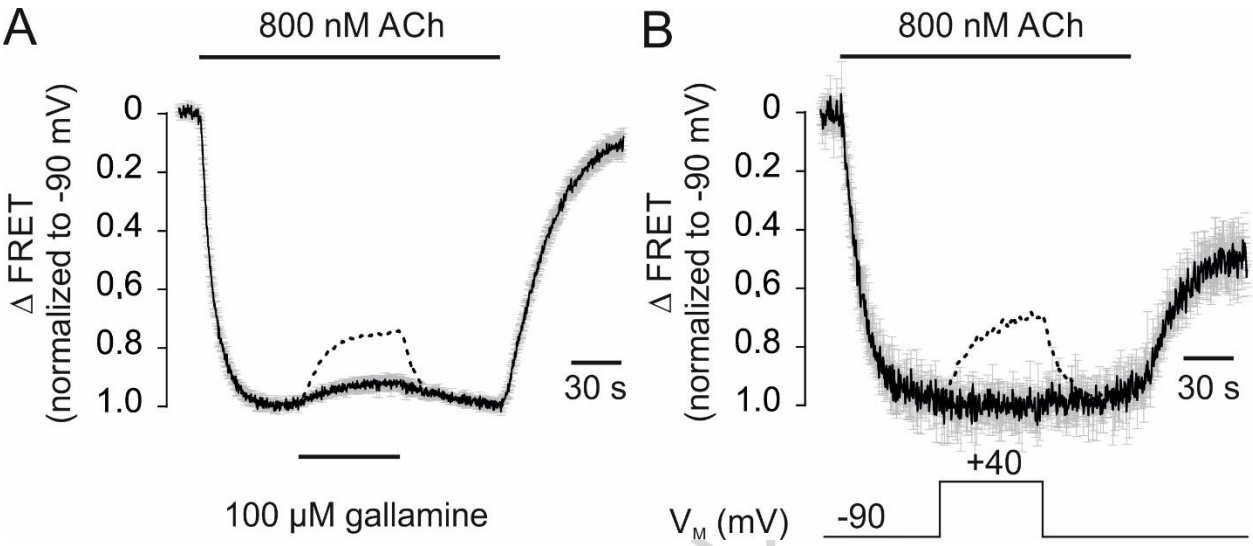

Figure 8:

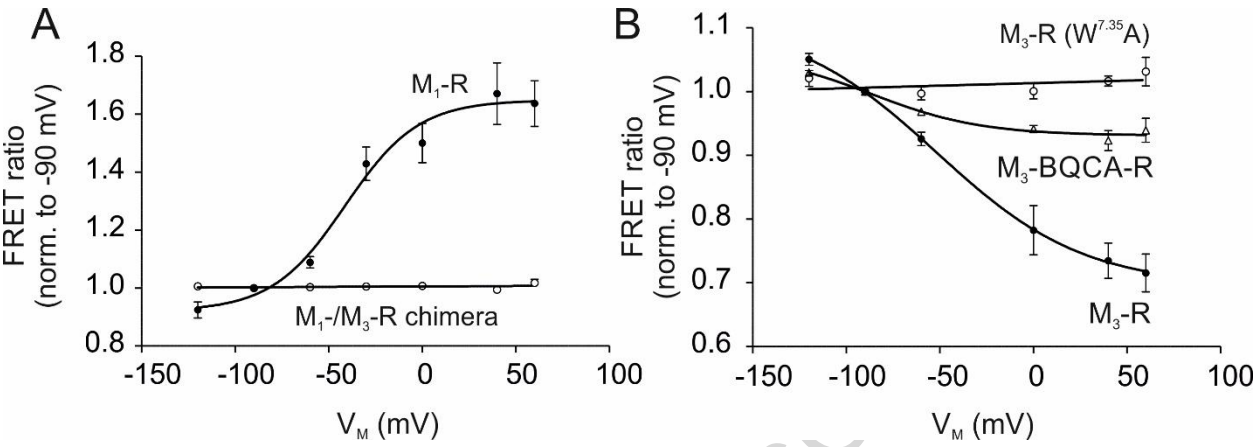

Figure 9

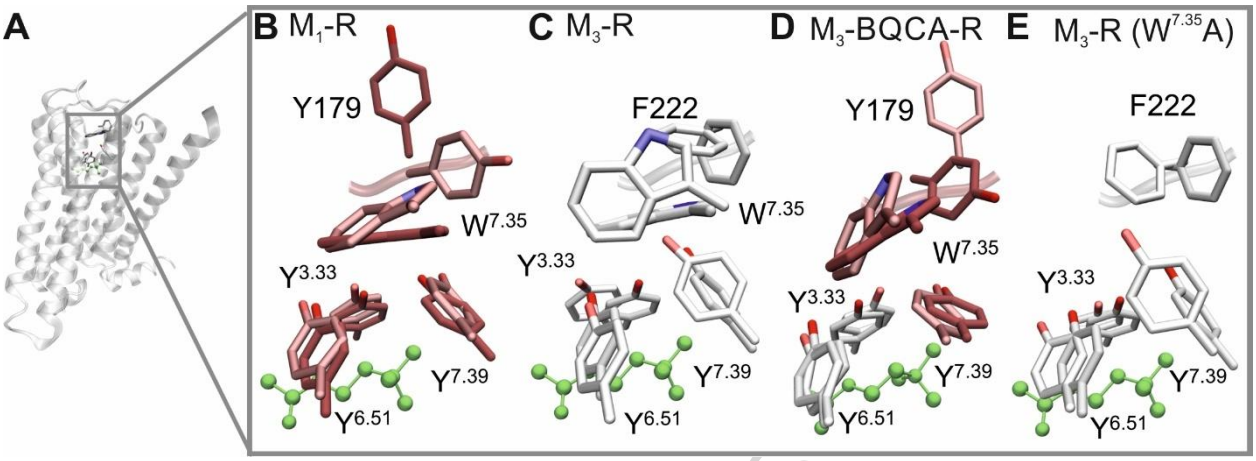

Figure 10

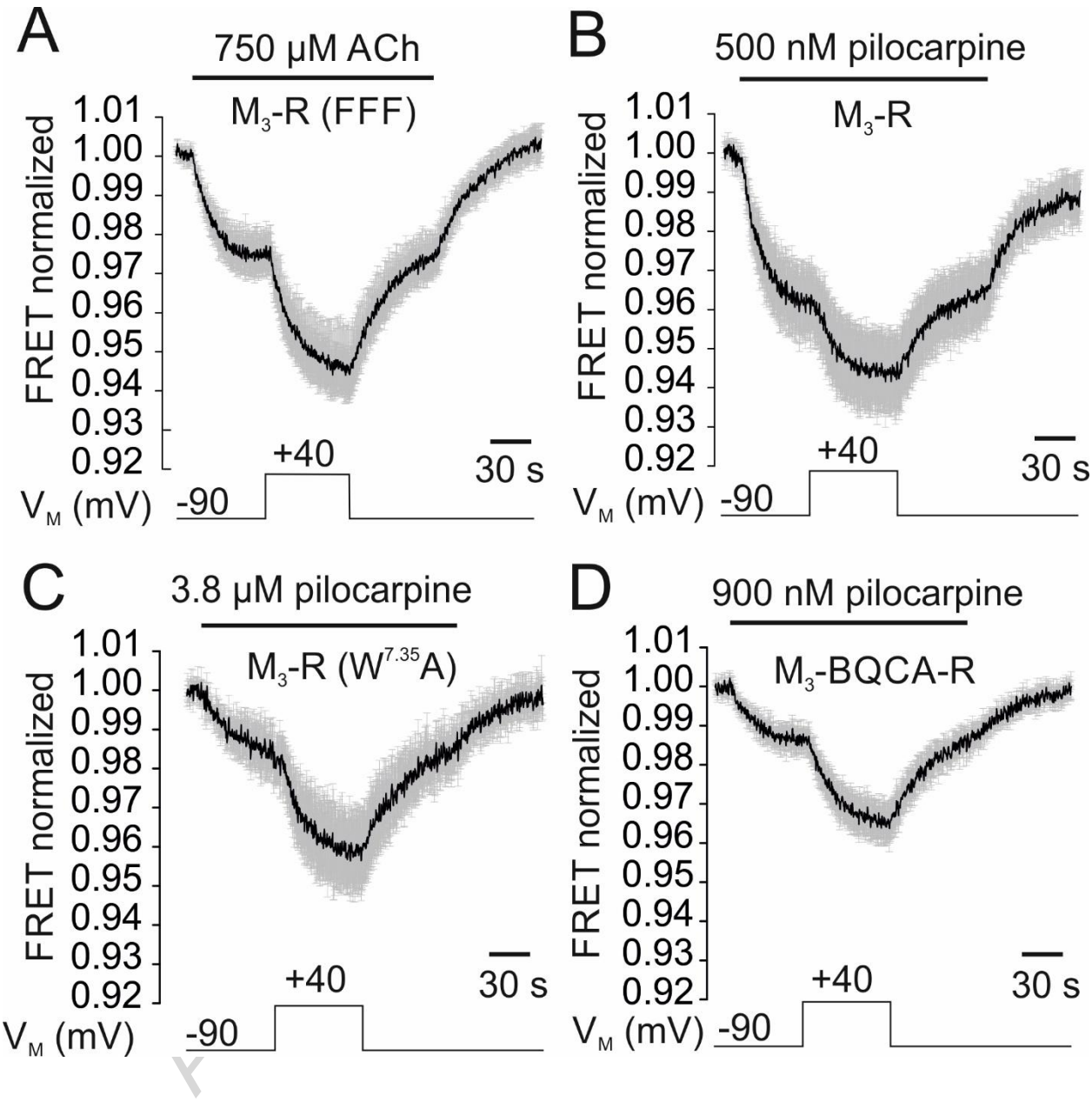

Highlights

- The allosteric site regulates voltage dependence of muscarinic receptors
- MD simulations identified a crosstalk between orthosteric and allosteric sites
- This crosstalk was specific for each muscarinic receptor subtype
- Our results explain differences in the voltage dependencies among muscarinic receptors